The Astrophysical Journal, 755:44 (12pp), 2012 August 10 doi:10.1088/0004-637X/755/1/44

IMPULSIVE ACCELERATION OF CORONAL MASS EJECTIONS. II. RELATION TO SOFT X-RAY FLARES AND FILAMENT ERUPTIONS

B. M. Bein[1], S. Berkebile-Stoiser[1], A. M. Veronig[1], M. Temmer[1], and B. Vršnak[2]
[1] Kanzelhöhe Observatory-IGAM, Institute of Physics, University of Graz, Universitätsplatz 5, A-8010 Graz, Austria
[2] Hvar Observatory, Faculty of Geodesy, University of Zagreb, Kačićeva 26, HR-10000 Zagreb, Croatia
Received 2012 February 24; accepted 2012 June 4; published 2012 July 25

ABSTRACT

Using high time cadence images from the *STEREO* EUVI, COR1, and COR2 instruments, we derived detailed kinematics of the main acceleration stage for a sample of 95 coronal mass ejections (CMEs) in comparison with associated flares and filament eruptions. We found that CMEs associated with flares reveal on average significantly higher peak accelerations and lower acceleration phase durations, initiation heights, and heights, at which they reach their peak velocities and peak accelerations. This means that CMEs that are associated with flares are characterized by higher and more impulsive accelerations and originate from lower in the corona where the magnetic field is stronger. For CMEs that are associated with filament eruptions we found only for the CME peak acceleration significantly lower values than for events that were not associated with filament eruptions. The flare rise time was found to be positively correlated with the CME acceleration duration and negatively correlated with the CME peak acceleration. For the majority of the events the CME acceleration starts before the flare onset (for 75% of the events) and the CME acceleration ends after the soft X-ray (SXR) peak time (for 77% of the events). In ∼60% of the events, the time difference between the peak time of the flare SXR flux derivative and the peak time of the CME acceleration is smaller than ±5 minutes, which hints at a feedback relationship between the CME acceleration and the energy release in the associated flare due to magnetic reconnection.

Key words: methods: statistical – Sun: coronal mass ejections (CMEs) – Sun: flares

Online-only material: color figures

1. INTRODUCTION

Solar flares and coronal mass ejections (CMEs) are the two most energetic phenomena in our solar system. Solar flares are abrupt releases of energy up to 10^{25} J within tens of minutes and can be observed in the whole electromagnetic spectrum from radio emission to γ-rays (e.g., Fletcher et al. 2011). CMEs are sporadic ejections of coronal material with velocities in the range of ∼100–3000 km s^{-1} (e.g., Yashiro et al. 2004; Gopalswamy et al. 2009). It is generally accepted that both CMEs and flares are different manifestations caused by magnetic reconnection in the solar corona, but the details of how both phenomena are related are still under investigation.

Various statistical studies using white-light coronagraphic observations showed positive correlations between the flare intensity and CME velocity (e.g., Moon et al. 2002; Vršnak et al. 2005; Yashiro & Gopalswamy 2009) or CME kinetic energy (Burkepile et al. 2004; Yashiro & Gopalswamy 2009). The temporal differences between the CME and the flare onset were found to be quite small. Michalek (2009) and Yashiro & Gopalswamy (2009) found a Gaussian distribution for the difference between the flare and CME onsets. According to Michalek (2009), the mean difference is 7 minutes. In these studies, linear back extrapolation of the CME height-time curve was used to estimate the CME start time. However, the CME onset times cannot be accurately determined by using only coronagraphic observations, which miss the early phase of the CME acceleration and propagation due to the occulter disk.

The CME kinematics typically shows three phases of evolution (Zhang et al. 2001). In the initiation phase, the CME rises with velocities of several tens of km s^{-1}, followed by an impulsive acceleration. Thereafter, the CME propagates with almost constant or slowly decreasing/increasing velocity depending on its interaction with the ambient solar wind (e.g., Gopalswamy et al. 2000). Recent case studies (e.g., Gallagher et al. 2003; Vršnak et al. 2004; Temmer et al. 2008) combined EUV images with coronagraphic observations to derive detailed CME acceleration profiles from the CME initiation close to the solar surface until its propagation beyond 15 $R_\odot$. In these events the CME acceleration profiles showed a good synchronization with the energy release in the associated flare, as evidenced in the hard X-ray (HXR) flux or soft X-ray (SXR) derivative. Maričić et al. (2004) studied a set of 22 CME events associated with flares using *SOHO* EIT, *MLSO* Mark IV, and *LASCO* C2 and C3. They report correlations between various CME and flare parameters as well as a close synchronization between the CME acceleration and the flare SXR flux derivative for ⩾50% of the events under study.

In Bein et al. (2011, hereafter Paper I), we presented statistics and correlations between various decisive CME parameters for a sample of 95 events: peak velocity, peak acceleration, acceleration duration, height at peak velocity, height at peak acceleration, and initiation height. To this aim we combined EUV images from the Extreme Ultraviolet Imager (EUVI; Wuelser et al. 2004) with COR1 and COR2 coronagraphic observations on board the *STEREO* mission. The high time cadence and the overlapping fields of view (FOVs) of the different *STEREO* instruments enabled us to derive detailed and continuous CME height-, velocity-, and acceleration-time profiles from the low corona up to about 15 $R_\odot$. Out of the 95 CMEs presented in Bein et al. (2011), 70 events could be associated with a *Geostationary Operational Environmental Satellite* (*GOES*) flare and 24 events with a filament eruption. Nine events are associated with both, a flare and a filament. In the present paper, we perform a statistical study on the relation between characteristic CME and flare parameters as well as on the temporal relationship between the two phenomena. We also study the characteristic CME parameters separately for events

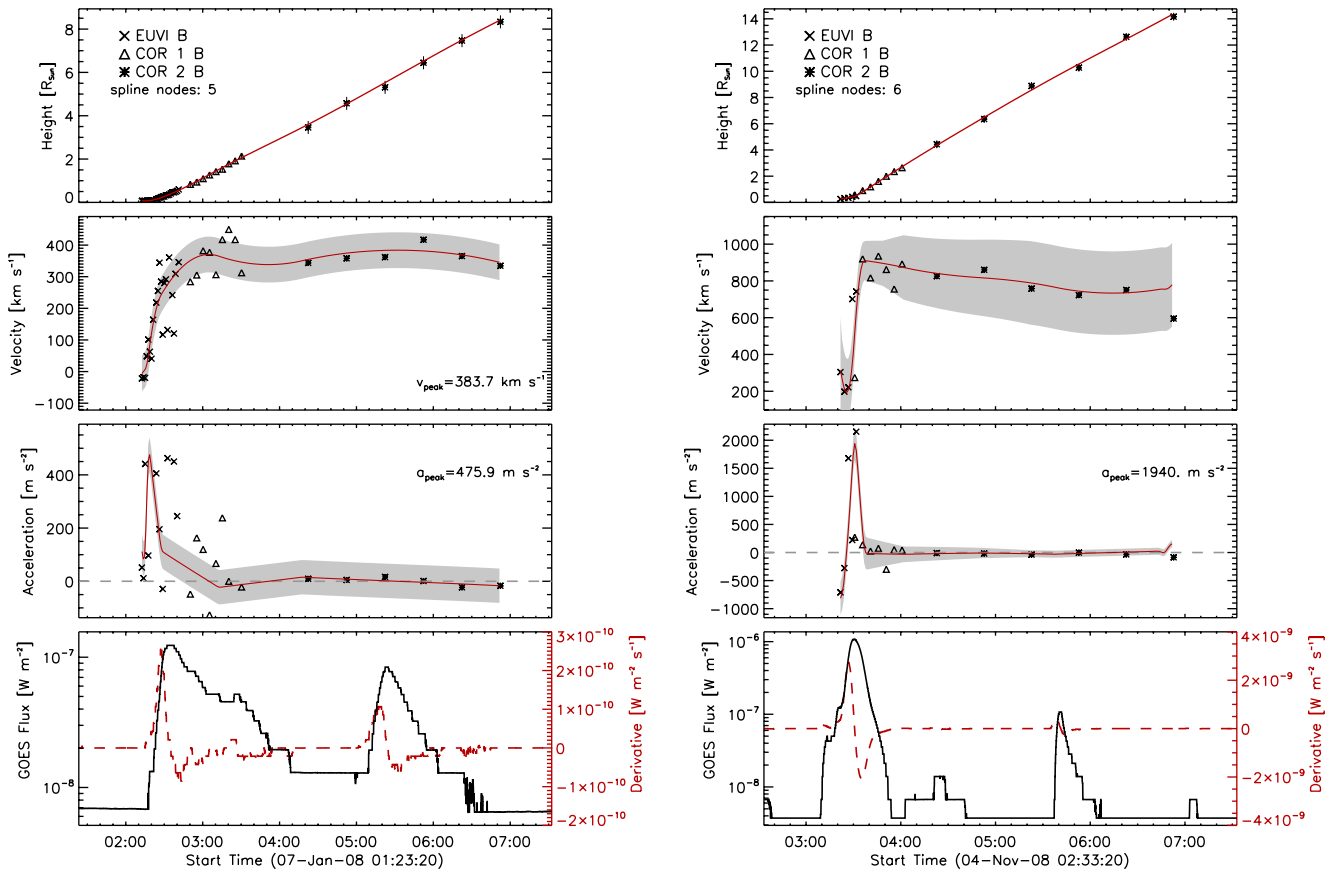

Figure 1. CME kinematics and *GOES* 1–8 Å soft X-ray flux for the CME–flare events that occurred on 2008 January 7 (left) and 2009 January 9 (right). The top panels show the measured CME height-time curve derived from *STEREO* EUVI (crosses), COR1 (triangles), and COR2 (asterisks) observations. The measurement errors (0.03 $R_\odot$ for EUVI, 0.125 $R_\odot$ for COR1, and 0.3 $R_\odot$ for COR2), which are in some cases smaller than the plot symbols, and the spline fit (solid line) are overplotted. The second and third panels show the CME velocity and acceleration profiles, derived from numerical differentiation of the direct measurements (plot symbols) and the spline fit (solid line) to the height-time curve. The gray shaded area represents the error range of the spline fit. The bottom panels show the *GOES* flux (black solid line) and its derivative (red dashed line) of the associated flare.

(A color version of this figure is available in the online journal.)

with/without associated flares and with/without associated filament eruptions.

2. DATA

The CME kinematics was derived from data of the *STEREO*/SECCHI instrument suite (Howard et al. 2008). The *STEREO* mission consists of two nearly identical spacecraft, *STEREO-A*, which moves ahead of the Earth, and *STEREO-B*, which moves behind the Earth. The SECCHI package consists of an EUVI, two coronagraphs (COR1 and COR2), and two Heliospheric Imagers (HI1 and HI2). For our study of the CME kinematics we combined data from EUVI, COR1, and COR2.

EUVI provides observations from the solar chromosphere and low corona in four different wavelengths with an FOV up to 1.7 $R_\odot$ (Wuelser et al. 2004). For our study we used primarily 171 Å observations with a time cadence as high as 75 s. In some cases it was only possible to track the CME in 195 Å observations with a default cadence of 10 minutes, but in some cases as good as 2.5 minutes. The high time cadence was necessary to derive detailed acceleration profiles of the CME initiation and impulsive acceleration phase. Observations in 171 Å and 195 Å were compared to 304 Å filtergrams to check if a filament eruption and/or flare were observed in association with the CME under study.

The inner coronagraph COR1 has an FOV of 1.4–4 $R_\odot$. For most events it has a nominal time cadence of 5 minutes, but in some cases it was also lower (20 minutes). The outer coronagraph COR2 has an FOV of 2.5–15 $R_\odot$ and an observing cadence of 30 minutes for the polarized brightness images, which were used in our study (Howard et al. 2008). The overlapping FOVs between EUVI and COR1 and between COR1 and COR2 made it possible to connect the same CME structure in all three instruments and thus to study the CME evolution continuously from its initiation close to the solar surface up to about 15 $R_\odot$. To compare the CME kinematics with the flare SXR evolution, we used *GOES* 1–8 Å flux measurements.

3. RESULTS

We studied 95 CMEs, which occurred between 2007 January and 2010 May, i.e., at the transition from solar cycle no. 23 to no. 24. For each event the full CME height, velocity, and acceleration profiles could be derived. For details on the methods applied we refer to Paper I. For each event, which was associated with a *GOES* flare, we compared the CME kinematics with the *GOES* SXR flux evolution and its derivative. Because of the temporal correlation between the HXR emission caused by flare-accelerated electron beams and the derivative of the SXR emission observed in many flare events (Neupert effect; Neupert 1968; Dennis & Zarro 1993; Veronig et al. 2002, 2005), we use the derivative of the *GOES* 1–8 Å flux as a proxy for the evolution of the flare energy release. Figures 1 and 2 show four

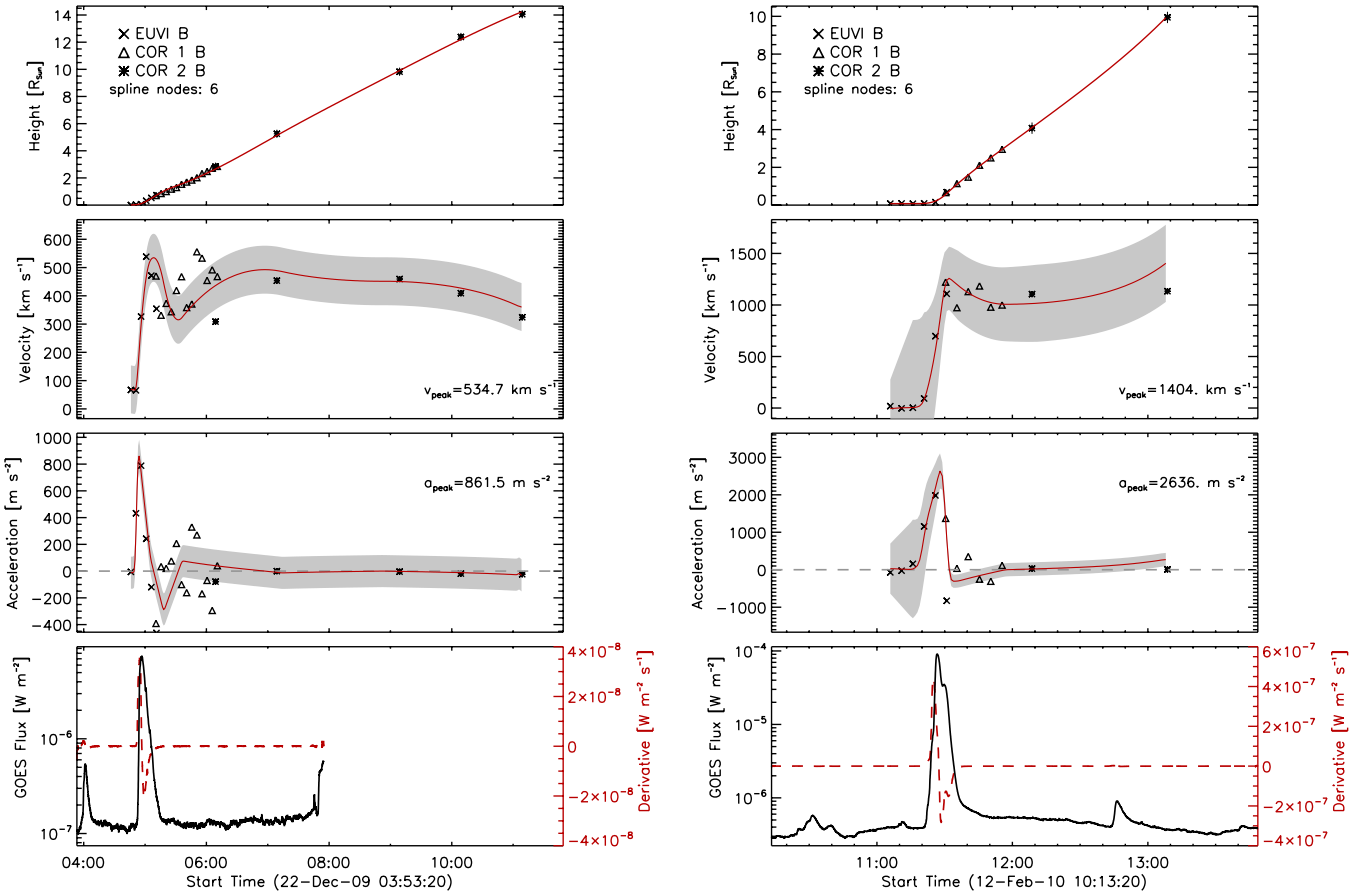

Figure 2. Same as Figure 1 but for the events observed on 2009 December 22 (left) and 2010 February 12 (right).
(A color version of this figure is available in the online journal.)

representative events of our sample. The top panels show the CME height, the second panels the CME velocity, and the third panels the CME acceleration curve against time. In the bottom panels the *GOES* 1–8 Å flux and its derivative are plotted.

For each CME we derived the following characteristic parameters: (1) peak velocity $v_{\rm max}$, (2) peak acceleration $a_{\rm max}$, (3) acceleration phase duration $t_{\rm acc}$, (4) first measured height h_0, (5) height at peak velocity $h_{v\rm max}$, and (6) height at peak acceleration $h_{a\rm max}$. We applied a spline fit to the CME height-time profile, and from its first and second derivative we derived $v_{\rm max}$ and $a_{\rm max}$, respectively. $a_{\rm max}$ is given by the maximum value of the CME acceleration profile; $v_{\rm max}$ is defined as the value of the velocity profile where the acceleration profile has decreased to 10% of its peak value. This definition is used in order to ensure that the peak velocity during the CME impulsive acceleration phase (Zhang et al. 2004) is calculated excluding the effect of the subsequent residual acceleration phase (for details see Paper I). The acceleration phase duration $t_{\rm acc}$ was defined as the time difference between $t_{\rm acc\_end}$, the time when the acceleration profile has decreased to 10% of its maximum value, and $t_{\rm acc\_start}$, the time in the increasing phase of the acceleration when the profile has reached 10% of its maximum value. h_0, the first measured height in our height-time plots, is used as a rough estimate of the CME initiation height, because we measured the CMEs as soon as it was possible to observe them in the low corona. The heights $h_{v\rm max}$ and $h_{a\rm max}$ are defined as the heights where the CME reached its peak velocity ($v_{\rm max}$) and peak acceleration ($a_{\rm max}$). A detailed study of these CME parameters is presented in Paper I.

3.1. CME Characteristics in Dependence of Flare/Filament Association

We studied each CME parameter ($v_{\rm max}$, $a_{\rm max}$, $t_{\rm acc}$, h_0, $h_{v\rm max}$, and $h_{a\rm max}$) separately for CMEs with/without associated flares and with/without associated filament eruptions. Figures 3–8 show the distributions of the different CME parameters for the whole sample of 95 events (gray histograms) together with the distribution for events associated with flares (colored histogram in the top panel) and for events associated with filament eruptions (colored histogram in the bottom panel). For each parameter we derived the arithmetic mean together with its standard deviation and the median and its absolute deviation, for the whole sample as well as separately for the samples with/without associated flares or filaments. The resulting values are summarized in Table 1. Because the distributions do not show a Gaussian behavior but have a tail toward high values, a lognormal distribution better describes their behavior (Limbert et al. 2001; Yurchyshyn et al. 2005; Bein et al. 2011). Thus, we also calculated the mean value μ and the standard deviation σ of the natural logarithm of the different CME parameter distributions (Cowan 1998):

$$\sigma = \sqrt{\ln\left(\frac{\rm Var}{E^2}+1\right)} \quad (1)$$

$$\mu = \ln(E) - \frac{\sigma^2}{2}, \quad (2)$$

Table 1
Statistical CME Parameters Derived for Different Subgroups

		All CMEs (95 Events)	With *GOES* Flare (70 Events)	Without *GOES* Flare (25 Events)	With Filament (24 Events)	Without Filament (71 Events)
v_{max} (km s^{-1})	mean ± s	526 ± 263	550 ± 268	459 ± 242	467 ± 227	546 ± 273
	median ± mad	460 ± 160	461 ± 150	393 ± 135	400 ± 121	461 ± 161
	$\mu \pm \sigma$	6.15 ± 0.22	6.20 ± 0.12	6.00 ± 0.25	6.04 ± 0.21	6.19 ± 0.22
a_{max} (m s^{-2})	mean ± s	757 ± 1034	896 ± 1148	367 ± 424	391 ± 380	880 ± 1152
	median ± mad	414 ± 246	556 ± 306	241 ± 134	266 ± 103	545 ± 321
	$\mu \pm \sigma$	6.10 ± 1.05	6.31 ± 0.97	5.48 ± 0.85	5.64 ± 0.66	6.28 ± 1.00
t_{acc} (minutes)	mean ± s	44.6 ± 60.4	33.9 ± 30.2	74.4 ± 102.0	63.1 ± 102.3	38.3 ± 36.1
	median ± mad	29.0 ± 14.5	26.0 ± 13.5	33.0 ± 14.5	35.0 ± 17.0	26.0 ± 16.0
	$\mu \pm \sigma$	3.28 ± 1.04	3.23 ± 0.58	3.77 ± 1.06	3.50 ± 1.29	3.33 ± 0.64
h_0 ($R_\odot$)	mean ± s	0.24 ± 0.29	0.19 ± 0.24	0.40 ± 0.35	0.31 ± 0.33	0.22 ± 0.28
	median ± mad	0.14 ± 0.08	0.12 ± 0.06	0.27 ± 0.16	0.23 ± 0.17	0.14 ± 0.07
	$\mu \pm \sigma$	−1.85 ± 0.88	−2.17 ± 0.99	−1.19 ± 0.57	−1.56 ± 0.77	−1.97 ± 0.93
h_{amax} ($R_\odot$)	mean ± s	0.53 ± 0.64	0.36 ± 0.37	0.99 ± 0.95	0.72 ± 0.87	0.46 ± 0.53
	median ± mad	0.26 ± 0.12	0.24 ± 0.10	0.52 ± 0.34	0.35 ± 0.21	0.26 ± 0.12
	$\mu \pm \sigma$	−1.10 ± 0.90	−1.38 ± 0.72	−0.34 ± 0.65	−0.79 ± 0.90	−1.20 ± 0.84
h_{vmax} ($R_\odot$)	mean ± s	1.56 ± 1.82	1.17 ± 1.48	2.26 ± 2.38	2.00 ± 2.42	1.28 ± 1.54
	median ± mad	0.78 ± 0.42	0.70 ± 0.35	1.05 ± 0.53	0.86 ± 0.40	0.76 ± 0.41
	$\mu \pm \sigma$	−0.09 ± 0.94	−0.32 ± 0.96	0.44 ± 0.75	0.24 ± 0.91	−0.21 ± 0.90

Notes. Arithmetic mean with standard deviation, median with median absolute deviation (mad), and mean value μ with standard deviation σ of the lognormal probability function of the following decisive CME parameters: peak velocity v_{max}, peak acceleration a_{max}, acceleration phase duration t_{acc}, height h_0 where the CME leading edge could be identified for the first time, height at peak acceleration h_{amax}, height at peak velocity h_{vmax}. Mean, median, and μ of all these parameters were derived for the whole sample of events (Column 3) and for several subgroups: events with associated flares (Column 4), events for which no flare could be associated (Column 5), events with associated filament eruptions (Column 6), events for which no filament eruptions could be associated (Column 7).

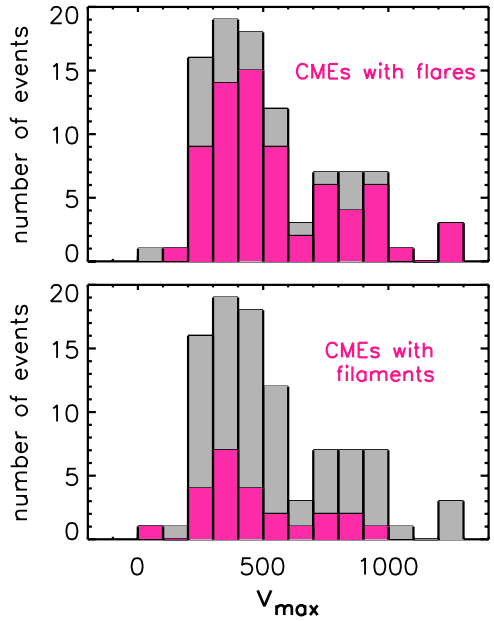

Figure 3. Histogram of the CME peak velocity v_{max} for the whole sample of 95 events (gray distributions in the top and bottom panels). In the top panel the v_{max} distribution of CME events associated with a flare is overlaid in color; in the bottom panel the histogram of CME events associated with an erupting filament is overlaid.

(A color version of this figure is available in the online journal.)

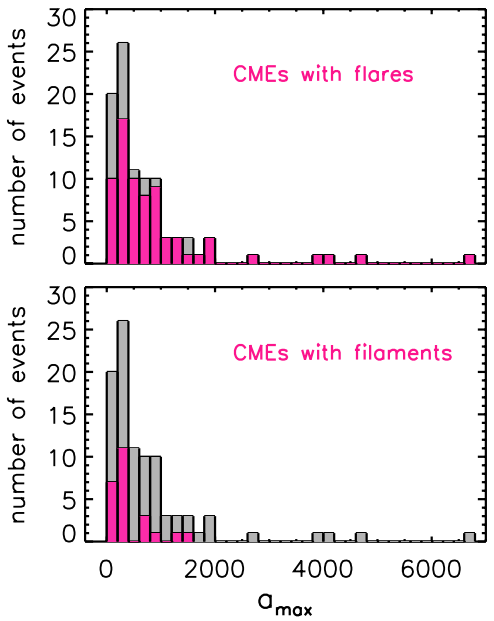

Figure 4. Same as Figure 3 but for the CME peak acceleration.

(A color version of this figure is available in the online journal.)

with E the mean value and Var the variance of the quantity. In the following we use $\mu^* = e^{\mu}$ and $\sigma^* = e^{\sigma}$ as the median and multiplicative standard deviation of the lognormal probability function of the distribution (Limbert et al. 2001). The confidence interval of 68.3% is given by $e^{\mu \mp \sigma}$; μ and σ are also summarized for each CME parameter in Table 1.

To check if the CME distributions with/without associated flares and with/without associated filament eruptions, respectively, come from the same continuous distribution (null hypothesis), we used the Kolmogorov–Smirnov test (e.g., Young 1977; Sachs 1997). This test is nonparametric, i.e., it

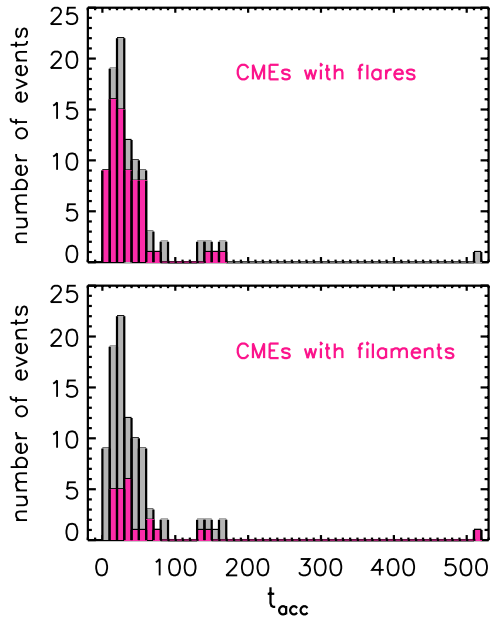

Figure 5. Same as Figure 3 but for the CME acceleration duration.
(A color version of this figure is available in the online journal.)

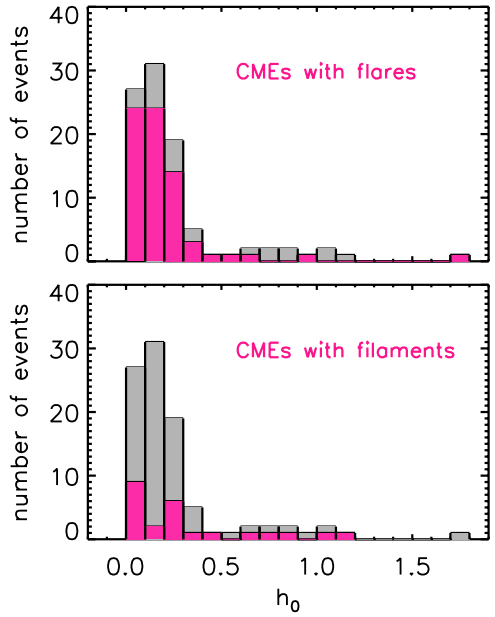

Figure 6. Same as Figure 3 but for the height h_0, where the CME could be first identified. This height is used as an estimate of the CME initiation height.
(A color version of this figure is available in the online journal.)

is not necessarily required to know the type of distribution (e.g., Gaussian, lognormal, exponential). A test statistic D is calculated by

$$D = \max \left| \frac{F_1}{n_1} - \frac{F_2}{n_2} \right|, \quad (3)$$

with F_1 and F_2 the cumulative distribution functions of both subsamples and n_1 and n_2 the number of events in each sample. D is then compared with

$$D_\alpha = K_\alpha \sqrt{\frac{n_1 + n_2}{n_1 \cdot n_2}}, \quad (4)$$

where K_α can be found in tables for different significance levels α. α represents the probability that we wrongly reject

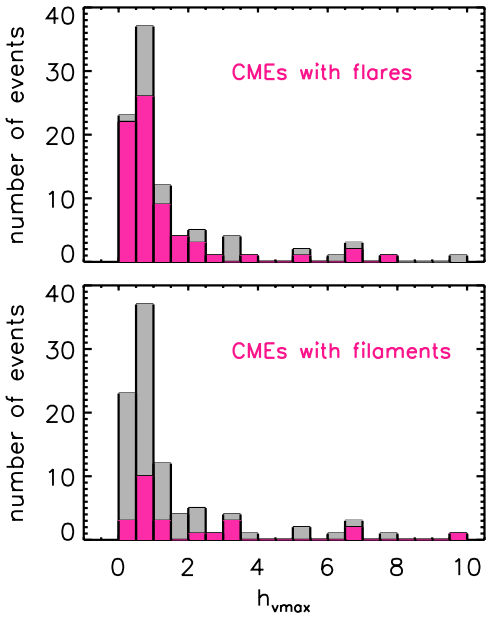

Figure 7. Same as Figure 3 but for the height $h_{v\max}$, where the CMEs reached their maximum velocity.
(A color version of this figure is available in the online journal.)

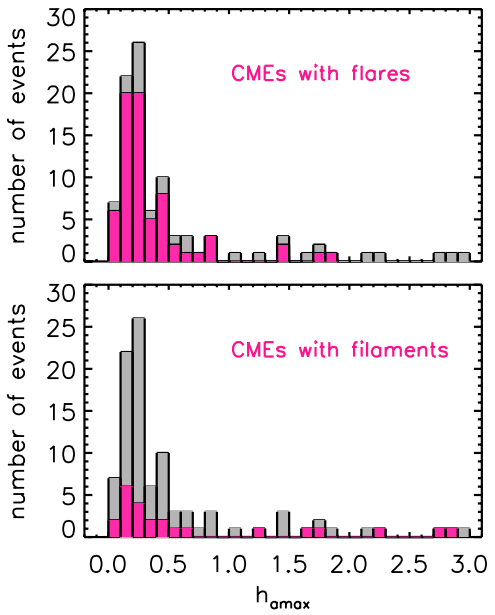

Figure 8. Same as Figure 3 but for the height $h_{a\max}$, where the CMEs reached their maximum acceleration.
(A color version of this figure is available in the online journal.)

the true hypothesis or accept the false hypothesis (Essenwanger 1976). If $D > D_\alpha$, the null hypothesis can be rejected, i.e., both subsamples do *not* come from the same population.

3.1.1. CME–Flare Relation

For 70 events out of our sample of 95 CMEs, we could identify an associated *GOES* class flare. Figure 9 shows the distribution of the *GOES* classes of the associated flares, which were not partially occulted (61 events): 9 events are associated with an A-class flare, 27 with a B-class flare, 20 events with a C-class flare, and 5 events with an M-class flare. None of the CME events under study are associated with an X-class flare.

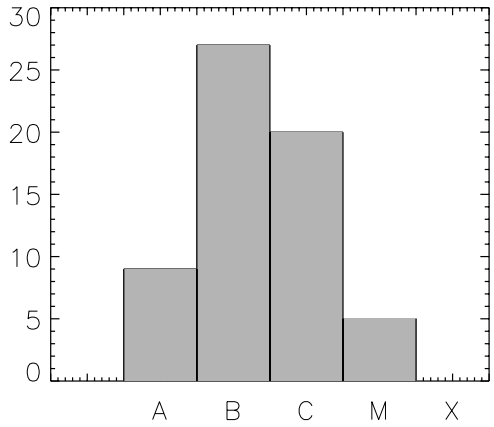

Figure 9. Distribution of the *GOES* classes of the flare events under study.

In the upper panels of Figures 3–8 the distributions of CMEs associated with flares (70 events) are overplotted in color. On average, the CME peak velocity $v_{\rm max}$ is higher for events associated with flares than for those with no flare association. Assuming a lognormal distribution, we find $\mu^* = 495^{-95}_{+117}$ km s^{-1} for events associated with flares and $\mu^* = 406^{-89}_{+113}$ km s^{-1} for events with no flare association. All CMEs, which reached a velocity higher than 1000 km s^{-1}, are associated with a flare. These results are in accordance with former studies. Burkepile et al. (2004), who measured the average velocity of 111 limb CMEs observed with the *Solar Maximum Mission* coronagraph/polarimeter, found mean values of 566 ± 67 km s^{-1} for CMEs with and 444 ± 59 km s^{-1} for CMEs without associated flares. Vršnak et al. (2005) analyzed the CME mean velocity and the velocity at a distance of 3 $R_\odot$ of CMEs using *LASCO* data and found for the flare-associated CME sample higher mean values than for the whole sample of CMEs. However, the Kolmogorov–Smirnov test applied to our sample does not show a clear distinction of both subsamples up to a significance level of 0.2.

For the CME peak acceleration $a_{\rm max}$ the differences in mean values and median values for events associated with flares and events with no flare association are even higher than for the velocities (see Table 1). We find a more than twice as high $\mu^* = 551^{-343}_{+904}$ m s^{-2} for events with flare-association than for CMEs without a flare, $\mu^* = 240^{-137}_{+321}$ m s^{-2}. Although the range of $a_{\rm max}$ values for flare–associated CMEs is large (77–6781 m s^{-2}), all events that reached a peak acceleration higher than 1600 m s^{-2} (9 events out of our sample of 95 CMEs) were associated with a flare. The Kolmogorov–Smirnov test, shows for the parameter $a_{\rm max}$ at a significance level of 0.05 that both distributions (with/without associated flare) do not come from the same population.

For the acceleration phase duration, we found $\mu^* = 25.3^{-11.2}_{+20.0}$ minutes for events with associated flares, compared to the $\mu^* = 43.8^{-28.6}_{+82.4}$ minutes for events with no associated flare. All CMEs with $t_{\rm acc} \leqslant 14$ minutes were associated with a flare. Applying the Kolmogorov–Smirnov test, it can be shown that both distributions do not come from the same population at a 0.10 significance level.

The measured CME height parameters h_0, $h_{v\rm max}$, and $h_{a\rm max}$ are on average smaller for CMEs associated with flares than for CMEs with no flare (see Table 1). μ^* of h_0 and $h_{v\rm max}$ are more than twice as high for events with no flare than for events with an associated flare. For μ^* of $h_{a\rm max}$ the differences between these subgroups are lower (ratio ∼1.32). The Kolmogorov–Smirnov test showed for all height parameters that both subgroups do not come from the same population at a significance level of 0.10 for h_0, 0.15 for $h_{v\rm max}$, and even 0.05 for $h_{a\rm max}$.

3.1.2. CME–Filament Relation

Twenty-four out of 95 CMEs were associated with an erupting filament. In the bottom panels of Figures 3–8 the distributions of these events are overplotted in color. Events that could be associated with filaments showed lower $v_{\rm max}$ than events without filament eruptions. For the former group we find $\mu^* = 420^{-67}_{+78}$ km s^{-1}, whereas for the latter group of CMEs we obtain μ^* of $v_{\rm max}$ of 531^{-107}_{+134} km s^{-1}. Burkepile et al. (2004) found no significant difference between both subgroups for the mean velocity of ∼520 km s^{-1}.

Similar to the CME–flare association, the differences in the mean and median values for $a_{\rm max}$ are more significant than for $v_{\rm max}$. CMEs that could be associated with filaments showed lower $a_{\rm max}$, with μ^* of 281^{-136}_{+264} m s^{-2}. None of these events reached $a_{\rm max}$ higher than 1600 m s^{-2}; 75% have $a_{\rm max} <$ 400 m s^{-2}. CME events without associated filament eruption show μ^* of 543^{-337}_{+915} m s^{-2}, i.e., the difference between these two subgroups is about a factor of two. $a_{\rm max}$ was the only parameter for which the Kolmogorov–Smirnov test suggested that both distributions (filament/non-filament associated events) do not come from the same population at a significance level of 0.05.

For the CME acceleration duration $t_{\rm acc}$ we found μ^* of $33.1^{-24.00}_{+87.00}$ minutes for events with associated filaments and μ^* of $27.8^{-13.10}_{+24.74}$ minutes for events with no filament association. Because filament eruptions are correlated to CMEs with larger $a_{\rm max}$, it is not surprising that they are also correlated to events with longer $t_{\rm acc}$, due to the strong negative correlation between $a_{\rm max}$ and $t_{\rm acc}$ (see Vršnak et al. 2007; Bein et al. 2011).

All CME height parameters h_0, $h_{v\rm max}$, and $h_{a\rm max}$ have on average larger values for CMEs associated with filament eruptions than for CMEs without filament eruptions (Table 1). The differences in the median values of the lognormal distribution are about a factor of 1.5.

Considering the mean and median values of CME parameters, we found higher values for $v_{\rm max}$ and $a_{\rm max}$ and smaller values for $t_{\rm acc}$, h_0, $h_{v\rm max}$, and $h_{a\rm max}$ for events with associated flares than for those with no flare. This effect is smallest for the CME peak velocity. The differences in the mean and median values show that CMEs associated with flares tend to have a more impulsive and intense acceleration and start from lower heights in the corona. CMEs that could be associated with an erupting filament behave oppositely. Their mean and median values of $v_{\rm max}$ and $a_{\rm max}$ are lower than for CMEs with no erupting filament, and the mean and median values of $t_{\rm acc}$, h_0, $h_{v\rm max}$, and $h_{a\rm max}$ are higher, when a filament eruption was associated. The Kolmogorov–Smirnov test shows for all CME parameters except $v_{\rm max}$ that the distributions of flare/non-flare-associated events do not come from the same population. Considering filament/non-filament events, the Kolmogorov–Smirnov test shows a distinction between both distributions only for $a_{\rm max}$.

3.2. Relationship between CME and Flare Parameters

We analyzed the scaling of the *GOES* peak flux $F_{\rm SXR}$ and the *GOES* SXR rise time $t_{\rm SXR}$ with the characteristics of the associated CMEs, i.e., $v_{\rm max}$, $a_{\rm max}$, $t_{\rm acc}$, h_0, $h_{v\rm max}$, and $h_{a\rm max}$, and calculated their dependency in logarithmic space. For these correlations we only considered those 61 (out of 70) flare events that were not partially occulted from Earth view. The

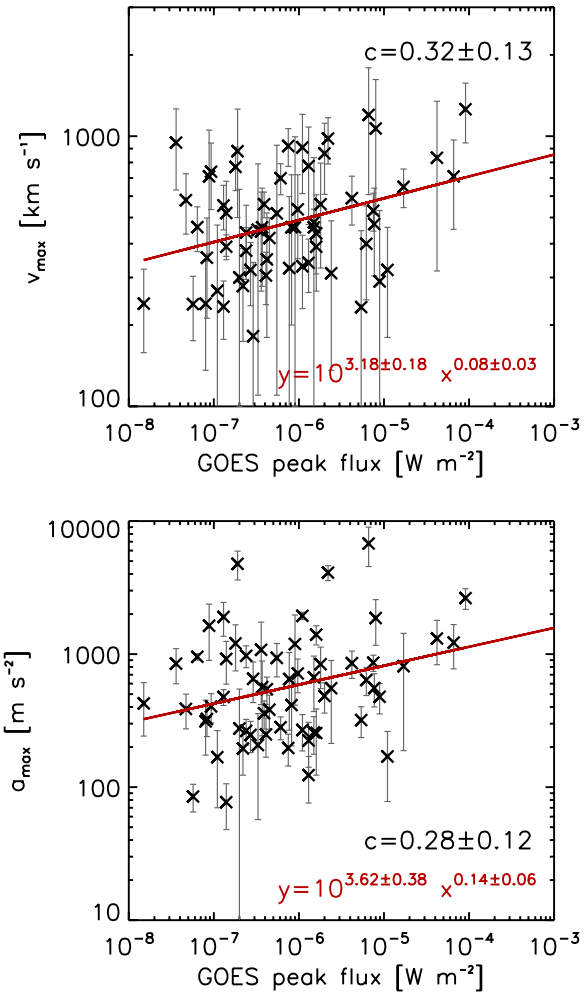

Figure 10. CME peak velocity (top) and peak acceleration (bottom) against the *GOES* peak flux of the associated flare. A double logarithmic space is used for the plot and the calculation of the correlation coefficient c, which is annotated in each panel. The regression line is overplotted in red.

(A color version of this figure is available in the online journal.)

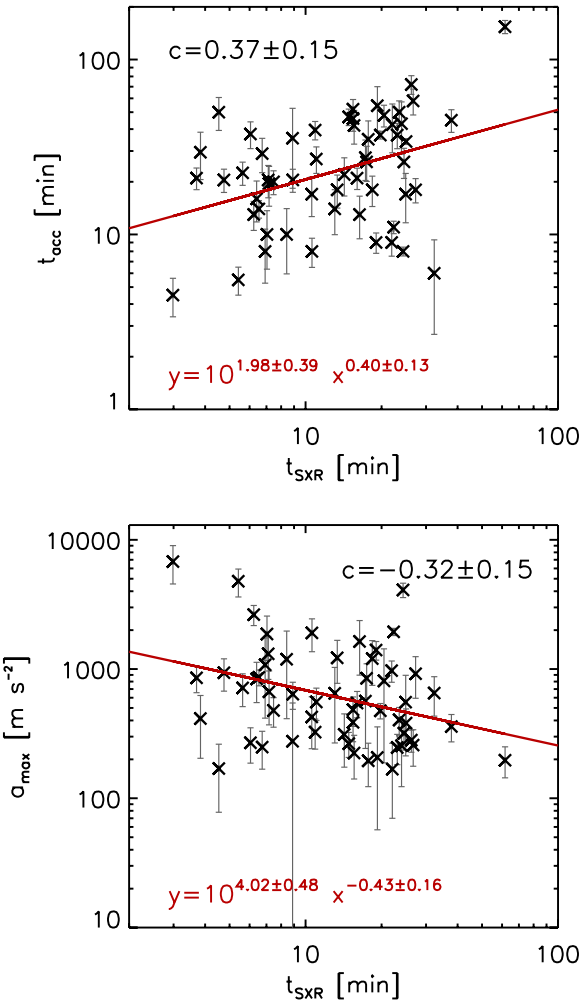

Figure 11. CME acceleration duration (top) and peak acceleration (bottom) against the flare SXR rise time. The correlation coefficient c (calculated in double logarithmic space) and the regression line are overplotted.

(A color version of this figure is available in the online journal.)

correlations are in general weak. Figures 10 and 11 show four representative correlations.

We used a bootstrap method (Efron 1979) within a Monte Carlo algorithm to estimate the standard error of our calculated correlation coefficients (Efron & Tibshirani 1986). A bootstrap sample is constructed by randomly drawing with replacement from the original data pairs, with the bootstrap sample having the same number of entries as the original sample. Such bootstrap samples are constructed 1000 times, and for each bootstrap sample the correlation coefficient is calculated. The mean value plus standard deviation of all 1000 calculations is used as a robust measure of the correlation coefficient and its standard error.

We found a positive correlation between $F_{\rm SXR}$ and $v_{\rm max}$ of $c = 0.32 \pm 0.13$ (bottom panel of Figure 10), i.e., CMEs that were associated with flares with higher SXR flux tend to reach higher peak velocities. This is consistent with the results from Maričić et al. (2007), who analyzed the correlation between SXR flares and CMEs for a set of 18 events, including B- to X-class flares, finding $c = 0.52$. The power-law dependency between $F_{\rm SXR}$ and $v_{\rm max}$ of our study can be expressed by

$$v_{\rm max} = 10^{3.18\pm0.18} F_{\rm SXR}^{0.08\pm0.03}. \quad (5)$$

The correlation between $F_{\rm SXR}$ and $a_{\rm max}$ is $c = 0.28 \pm 0.12$ (see the top panel of Figure 10), i.e., CMEs with high peak accelerations tend to be associated with flares of high *GOES* SXR flux. Maričić et al. (2007) also found a positive correlation between these two parameters with a correlation coefficient of $c = 0.60$. We found a power-law dependency of

$$a_{\rm max} = 10^{3.62\pm0.38} F_{\rm SXR}^{0.14\pm0.06}. \quad (6)$$

We determined the SXR rise time $t_{\rm SXR}$ from the derivative of the *GOES* flux curves as the time difference between the start of the increase and the maximum of the SXR derivative, which was possible for 57 events. The distribution of the time differences is shown in Figure 12. The *GOES* SXR rise time $t_{\rm SXR}$ and CME parameters (Figure 11) do not yield distinct correlations. The highest correlation coefficient was obtained for the relation between $t_{\rm SXR}$ and the CME acceleration duration, $c = 0.37 \pm 0.15$. The power-law dependency between these two parameters can be expressed as

$$t_{\rm acc} = 10^{1.98\pm0.39} t_{\rm SXR}^{0.40\pm0.13}. \quad (7)$$

Between $a_{\rm max}$ and $t_{\rm SXR}$ we found a negative correlation with $c = -0.32 \pm 0.15$ and a power-law dependency of

$$a_{\rm max} = 10^{4.02\pm0.48} t_{\rm SXR}^{-0.43\pm0.16}, \quad (8)$$

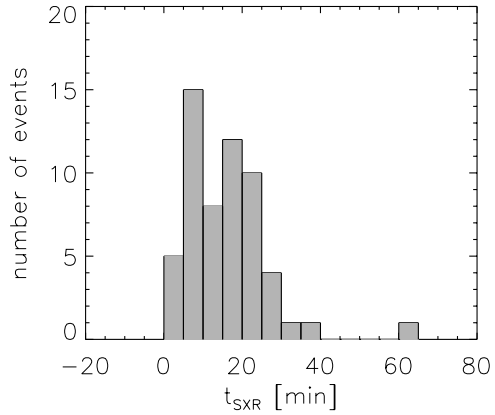

Figure 12. Distribution of the rise time t_{SXR} of the *GOES* SXR flares.

Table 2
Mean Value with Standard Deviation and Median with the Median Absolute Deviation (mad) of the CME Parameters v_{max}, a_{max}, t_{acc}, h_0, h_{vmax}, and h_{amax}, Separately for the Flare *GOES* Classes

		A-class (9 Events)	B-class (27 Events)	C-class (20 Events)	M-class (5 Events)
v_{max}	mean ± s	501 ± 258	532 ± 257	609 ± 301	754 ± 340
	median ± mad	461 ± 221	460 ± 135	530 ± 200	710 ± 122
a_{max}	mean ± s	597 ± 474	986 ± 1236	1229 ± 1489	1230 ± 906
	median ± mad	404 ± 92	639 ± 370	810 ± 502	1221 ± 411
t_{acc}	mean ± s	32.6 ± 15.6	28.9 ± 24.1	25.2 ± 15.7	29.9 ± 17.7
	median ± mad	26.0 ± 13.0	21.0 ± 12.0	20.5 ± 9.5	20.5 ± 7.5
h_0	mean ± s	0.22 ± 0.19	0.19 ± 0.27	0.14 ± 0.19	0.27 ± 0.39
	median ± mad	0.19 ± 0.09	0.11 ± 0.05	0.10 ± 0.05	0.11 ± 0.03
h_{vmax}	mean ± s	1.03 ± 0.62	0.89 ± 1.01	0.70 ± 0.47	0.80 ± 0.65
	median ± mad	1.30 ± 0.61	0.70 ± 0.28	0.61 ± 0.21	0.70 ± 0.20
h_{amax}	mean ± s	0.41 ± 0.28	0.31 ± 0.33	0.31 ± 0.32	0.58 ± 0.58
	median ± mad	0.33 ± 0.17	0.23 ± 0.08	0.22 ± 0.10	0.27 ± 0.13

i.e., CMEs with high peak accelerations are preferentially associated with flares, which show short SXR rise times.

One possible explanation for the weak flare–CME correlations we obtained is the lack of strong flare events in our sample, which contains only a few M-class flares and no X-class flares due to the solar activity minimum condition in the period under study (2007–2010). Since we cover only low energetic flares and thus a relatively narrow range of *GOES* classes, possible correlations may be hidden in the scatter of the data points. It turned out that weak flares show a larger scatter in the distribution of values, which weakens our correlation results since predominantly A- and B-class flares are studied in our sample. To circumvent this effect, we calculated the mean and median value of the CME parameters separately for each *GOES* class (shown in Table 2). By this procedure the CME parameters were weighted for each *GOES* class equally, which reduced the influence of the scattering of the large number of A- and B-class flares in our sample.

Figure 13 shows these mean values for v_{max}, a_{max}, and t_{acc} plotted against the mean *GOES* flux of each subgroup. In this representation a clear trend is noticeable that CMEs, which reach higher peak velocities, are related to flares with higher *GOES* peak flux (top panel in Figure 13), consistent with former studies. Moon et al. (2002) analyzed 3217 *LASCO* CMEs that were associated with flares and compared the median value of the CME speeds derived from the whole sample, from CMEs associated with flares >C1, and from CMEs associated with flares >M1. When considering the whole sample, the

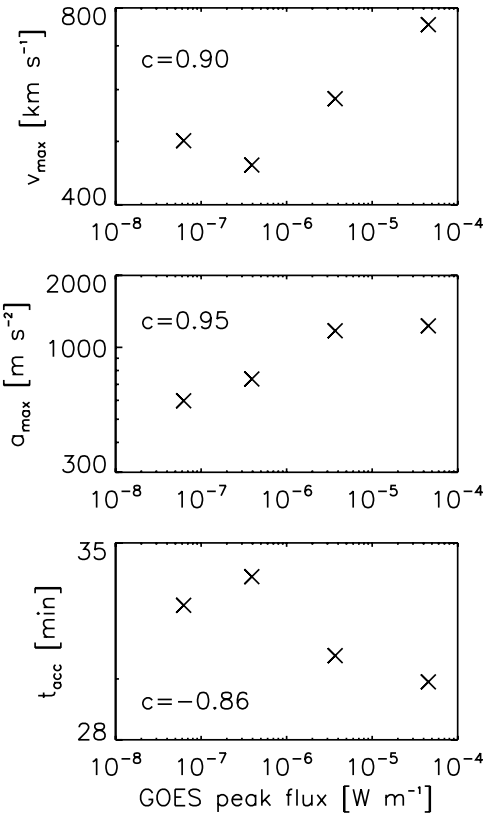

Figure 13. Mean value of the CME peak velocity v_{max} (top), acceleration a_{max} (middle), and acceleration duration t_{acc} (bottom) for each *GOES* class plotted against the mean *GOES* flux in each subgroup. The correlation coefficient c (calculated in logarithmic space) is annotated in each panel.

authors found the lowest median value, whereas CMEs that were associated with flares >M1 showed the largest median value for the CME speed distribution. Vršnak et al. (2005) compared the velocities between B and C flare-associated CMEs with the velocities of M- and X-class flare-associated CMEs and found that the mean value of the M- and X-class flare-associated events is about 1.4 times the mean value of the other subgroup.

We also find that the mean values of the CME peak acceleration are positively correlated with the *GOES* peak flux (middle panel of Figure 13). The bottom panel of Figure 13 shows the mean values of the CME acceleration duration against the *GOES* peak flux, which shows a tendency that t_{acc} is smaller for CMEs associated with higher energetic flares. The mean and median values calculated for each *GOES* class separately for all CME parameters under study are summarized in Table 2.

3.3. Flare–CME Temporal Relationship

We studied the relative timing of the CME acceleration phase and the flare energy release in order to investigate possible temporal synchronizations between these two phenomena. From the CME observations we derived the start (t_{acc_start}), peak (t_{acc_peak}), and end time (t_{acc_end}) of the CME acceleration. From the *GOES* flare observations we derived the start and peak time of the 1–8 Å SXR flux as well as the peak of the 1–8 Å flux derivative. For this study we used only flare events that were not partially occulted and for which a peak in the derivative of the *GOES* flux could be derived. This was the case for 57 out of 70 flare–CME pairs.

The top panels of Figure 14 show the histograms of the time differences between the *GOES* flare start times and the start of

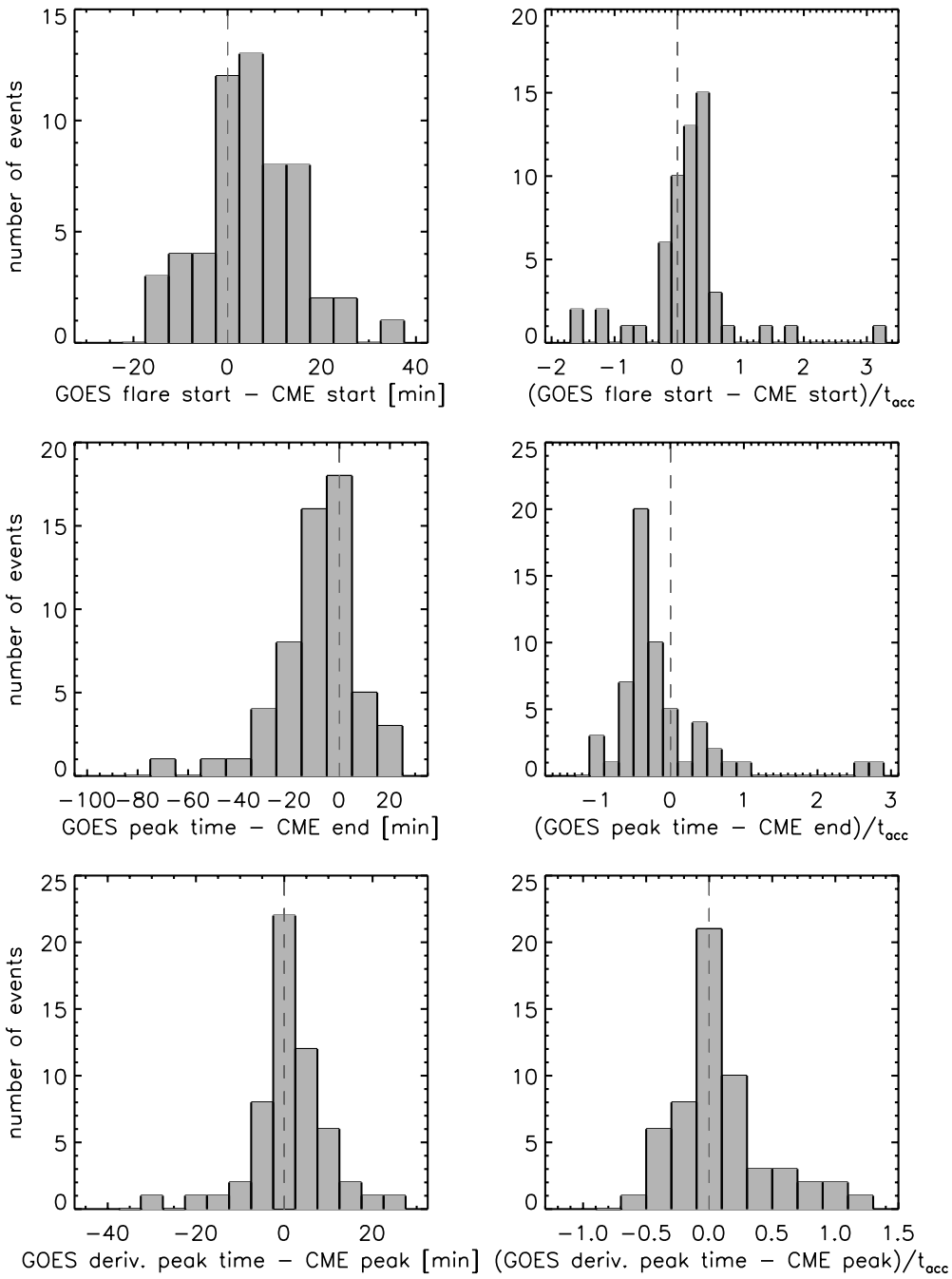

Figure 14. Distribution of the time differences between the start of the *GOES* flare and the start of the CME acceleration (top), *GOES* peak time and CME acceleration end time (middle), and the peak time of the derivative of the *GOES* 1–8 Å flux and the CME acceleration peak time (bottom). On the left-hand side the time differences are plotted in minutes, whereas on the right-hand side the time differences are normalized by the acceleration duration of the corresponding CMEs. Positive values mean that the CME acceleration start, end, or peak occurred before the flare SXR start, peak, or derivative peak, respectively.

the associated CME acceleration. For the distribution on the left-hand side the differences expressed in minutes were used, whereas the values on the right-hand side were normalized by the CME acceleration duration. For the time differences we found a mean value of 4.9 ± 10.2 minutes and a median of 4.6 ± 6.3 minutes. The distribution shows that the values are confined to within about ±20 minutes (93% of the events lie within this interval). In 75% of the cases, the time difference is positive, i.e., the CME acceleration starts *before* the rise of the flare SXR flux. Considering the normalized values, the time difference is smaller than ±0.5 for 77% of the events and smaller than ±0.25 for 44%. Maričić et al. (2007) also found that for the majority of the events the CME acceleration starts before the SXR flare with a mean value of 23 ± 30 minutes (for a set of 18 events containing a significant fraction of gradual events). This mean value is larger than in our study, but the time delays normalized by t_{acc} are quite similar in both studies, with a mean value of 0.17 ± 0.71 in our study and 0.14 ± 0.20 in Maričić et al. (2007).

In the middle panels of Figure 14 we compare the end of the CME impulsive acceleration phase t_{acc_end} with the *GOES* SXR flare peak time, which relates to the end of the impulsive flare energy release phase. We found that for the majority of the events (77%), the *GOES* peak occurred earlier than t_{acc_end}. The

Table 3
Statistical Parameters Derived for Characteristic CME–Flare Time Differences

Time Delay	Minimum	Maximum	Arithmetic Mean ± Standard Deviation	Median ± Mad
GOES flare start time − t_{acc_start} (minutes)	−17.3	32.6	4.9 ± 10.2	4.6 ± 6.3
(*GOES* flare start time − t_{acc_start})/t_{acc}	−1.58	3.26	0.17 ± 0.71	0.17 ± 0.20
GOES flare peak time − t_{acc_end} (minutes)	−71.5	21.5	−9.3 ± 15.8	−6.5 ± 7.5
(*GOES* flare start time − t_{acc_end})/t_{acc}	−1.08	2.83	−0.13 ± 0.69	−0.33 ± 0.20
GOES der. peak time − t_{acc_peak} (minutes)	−31.5	23.0	1.29 ± 8.63	1.00 ± 4.00
(*GOES* der. peak time − t_{acc_peak})/t_{acc}	−0.63	1.17	0.09 ± 0.38	0.02 ± 0.18

Notes. Statistical parameters (minimum value, maximum value, arithmetic mean, standard deviation, median, and median absolute deviation) for time delays between characteristic CME and flare times: time difference between the start of the *GOES* flare and the start of the CME acceleration t_{acc_start} (differences expressed in minutes in the first row, values normalized by the CME acceleration time t_{acc} in the second row), time delay between the *GOES* flare peak time and the end of the CME acceleration phase t_{acc_end} (delays expressed in minutes in the third row, normalized values in the fourth row), and time difference between the peak time of the *GOES* derivative and the peak time of the CME acceleration t_{acc_peak} (delays expressed in minutes in the fifth row, normalized values in the sixth row).

mean value of the distribution is −9.3 ± 15.8 minutes and the median −6.5 ± 7.5 minutes. For some gradual CMEs (t_{acc} > 50 minutes), the delay between flare peak and acceleration end can be >30 minutes (three events). At the right-hand side the normalized difference between the *GOES* peak flux and t_{acc_end} is plotted. The distribution shows an asymmetric behavior with a tail at positive values and a distinct mode in the range of −0.5 to −0.3. For 65% of the events, the normalized time differences are between −0.7 and −0.1.

The time difference between the peak of the *GOES* 1–8 Å flux derivative and the CME acceleration peak (bottom left panel of Figure 14) is found to be small. The distribution does strongly peak around zero; for the mean value we obtained 1.3 ± 8.6 minutes, for the median 1.0 ± 4.0 minutes. Maričić et al. (2007), who used the logarithmic derivative of the SXR *GOES* flux, found a mean value of 2.7 ± 14 minutes, consistent with our findings. In 81% of the events, we found a difference smaller than ±10 minutes and for 58% of the events it is smaller than ±5 minutes. Only one event of our study showed a time delay >20 minutes. Sixty-five percent of the normalized values (distribution shown at the right-hand side of Figure 14) lie within ±0.25. The statistical parameters for the time differences described above are summarized in Table 3.

These findings provide strong evidence that the timing of the flare energy release and the CME dynamics (acceleration) are well synchronized, supporting previous results from case studies (e.g., Zhang et al. 2004). Recent studies also analyzed the relationship between the flare HXR emission and the CME acceleration peak, finding that the flare HXR peak occurs close in time with the maximum CME acceleration (Temmer et al. 2008, 2010; Cheng et al. 2010; Berkebile-Stoiser et al. 2012).

4. SUMMARY AND CONCLUSION

Based on a sample of 95 CME events, we present a statistical study on various characteristic CME parameters and their relation to flares. CMEs that are associated with flares show on average higher peak velocities (v_{max}), higher peak accelerations (a_{max}), shorter acceleration phase durations (t_{acc}), lower heights at peak velocity (h_{vmax}), lower heights at peak acceleration (h_{amax}), and lower initiation heights (h_0). The ratio between the median values of the lognormal probability functions of both subgroups is about a factor of two. Only for v_{max} is the ratio significantly smaller (∼1.1), most probably due to the small range of v_{max} values. Due to the anticorrelation between a_{max} and t_{acc} and the relation $v_{max} \approx a_{max} \cdot t_{acc}$, the range for v_{max} is smaller than for the other two quantities; it basically covers only one order of magnitude. Although we found clear differences in the mean and median values of the two subgroups, there exist also events associated with flares that have low v_{max} and a_{max} values and high t_{acc}, h_{vmax}, h_{amax}, and h_0. For instance, the smallest measured a_{max} value for a CME with flare was 77 m s^{-2}, and the highest measured value for a CME without flare was 1577 m s^{-2}. The Kolmogorov–Smirnov test suggested a distinction between both distributions (flare/non-flare-associated events) for every CME parameter (except for v_{max}) at 0.05–0.15 levels of significance. The clearest distinctions were found for a_{max} and h_{amax} at a 0.05 level of significance.

CMEs that are associated with erupting filaments show on average smaller v_{max} and a_{max} and larger t_{acc}, h_{vmax}, h_{amax}, and h_0. These trends are the opposite of those for the flare association. The ratio between the mean and median values of both subgroups is somewhat smaller than for the flare association. Again we found the smallest ratio between the median values μ^* of v_{max} (1.1). The μ^* of a_{max} and h_{vmax} showed the highest ratio with 1.9. For t_{acc}, h_{amax}, and h_0 we found ratios between 1.2 and 1.5. But there exist also CMEs associated with filament eruptions that have high v_{max} and a_{max} values and low t_{acc}, h_{vmax}, h_{amax}, and h_0. For example, the highest measured a_{max} value for a CME that was associated with an erupting filament was 1561 m s^{-2}, while the smallest value for a CME event with no erupting filament was 35 m s^{-2} (the second lowest value of the whole distribution). Both of these events were not associated with a flare. The Kolmogorov–Smirnov test did not show a clear distinction between both subgroups. Only for a_{max} did the test suggest that both distributions do not come from the same population at a 0.05 level of significance.

The correlations obtained between v_{max}, a_{max}, and t_{acc} with the *GOES* peak flux F_{SXR} and the SXR rise time t_{SXR} of the associated flare were low. We found a weak positive correlation between the CME acceleration duration t_{acc} and the flare rise time t_{SXR} ($c = 0.37 \pm 0.15$) and a weak negative correlation between a_{max} and t_{SXR} ($c = -0.32 \pm 0.15$). Correlations between v_{max} and a_{max} with F_{SXR} were $c = 0.32 \pm 0.13$ and $c = 0.28 \pm 0.12$, respectively. If the events are averaged and binned into the different *GOES* classes, the correlations are much more distinct. The mean values in each *GOES* class show an increasing trend for v_{max} and a_{max} and a decreasing trend for t_{acc} with higher *GOES* flux.

For the majority of the events (75%) we found that the CME acceleration starts *before* the SXR flare onset, which is

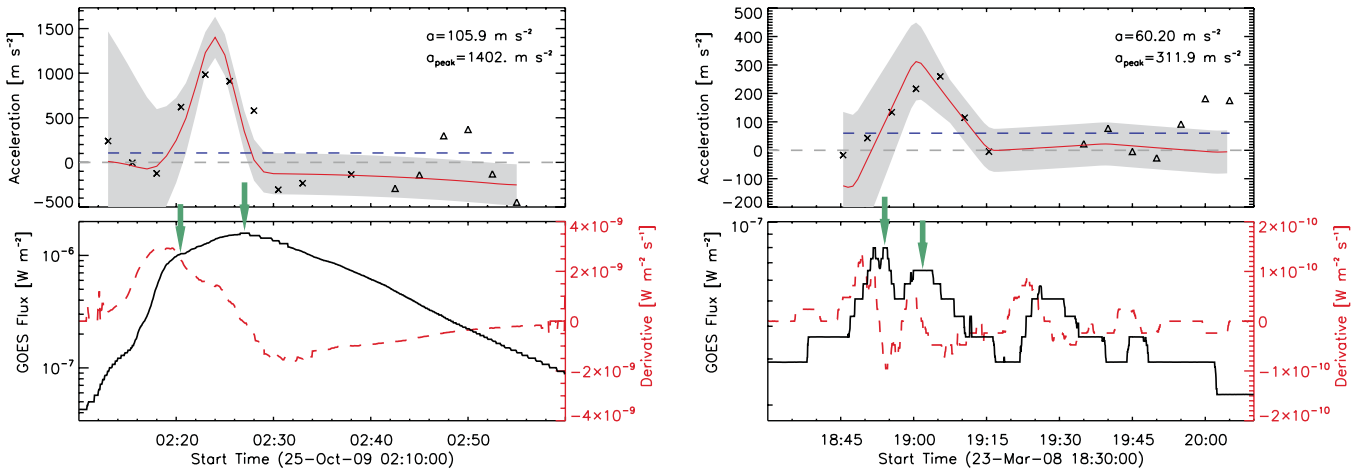

Figure 15. CME acceleration (top) and *GOES* SXR curve (bottom) from the events observed on 2009 October 25 (left) and 2008 March 23 (right). In both events the CME acceleration starts after the flare onset, which may be related to an overlap of two flares. Arrows mark two SXR maxima indicating two possible flare maxima.

(A color version of this figure is available in the online journal.)

consistent with the findings of Maričić et al. (2007), suggesting that the flare is a consequence of the eruption. Similar to our study, these authors also found about one-fourth of the events for which the onset of the associated flare occurred before the CME acceleration started. They explained these cases by a superposition of two flares, a confined flare in the pre-eruption stage, which releases only a part of the stored magnetic energy, and a second flare, beginning after the CME acceleration onset and causing a prolongation of the first flare in the full-disk integrated SXR light curve. The CME is associated with the second flare, but because of the superposition, the flare start is measured from the first one. To test this hypothesis, we checked the SXR curves for all events for which the CME acceleration start was after the flare onset and found indeed in 11 out of 14 events evidence of a second SXR peak, confirming their suggestion.[3] Figure 15 shows two representative examples. The top panels show the CME acceleration profile, the bottom panels the *GOES* SXR flux together with its derivative. We marked the two possible SXR peaks by arrows. Assuming that we have a superposition of two subsequent flares, we would also measure erroneous SXR start times and, as a result, too long t_{SXR}. This misidentification would also influence our correlation negatively. To test this, we correlated t_{SXR} again with a_{max} and t_{acc} considering only events for which the CME acceleration starts before the flare onset and found indeed distinctly higher correlation coefficients (Figure 16, $c = 0.59 \pm 0.12$ and $c = -0.50 \pm 0.14$) than for the whole sample (shown in Figure 11, $c = 0.37 \pm 0.15$ and $c = -0.32 \pm 0.15$). Thus, a superposition of two subsequent flares and more complex structures are probably a reason for the weak correlations and may account for a considerable number of events where the flare seems to start before the eruption.

For the majority of the events (77%) we found that the end of the CME acceleration occurred *after* the SXR peak. Especially long duration flares reach a certain point when they become too weak to compensate cooling of the hot plasma. As a result, the SXR curve decreases although the energy release in the flare may still be going on.

For 81% of the events the time delay between the CME acceleration peak and the peak of the *GOES* SXR flux derivative,

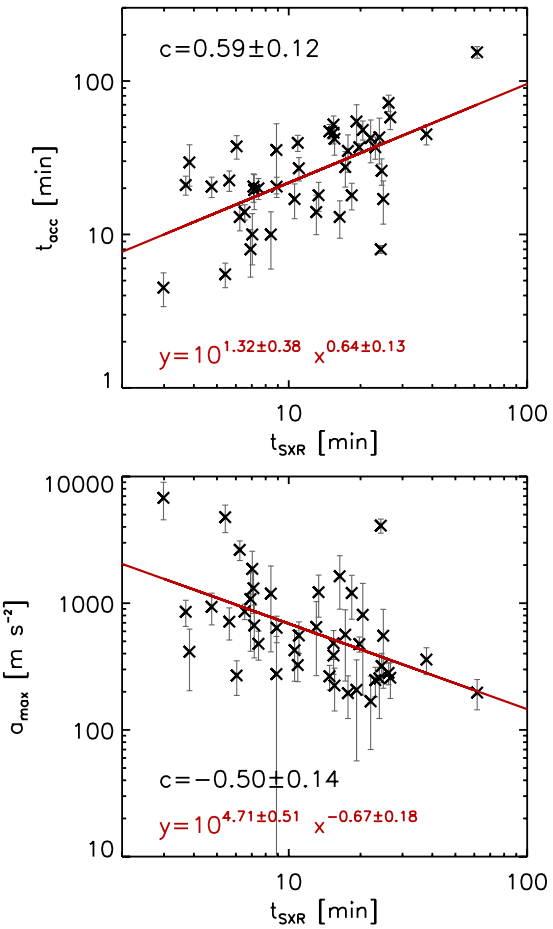

Figure 16. Same as Figure 11 but only for events where the CME acceleration starts before the flare.

(A color version of this figure is available in the online journal.)

which is a proxy for the flare energy release rate, was smaller than ±10 minutes, for 58% smaller than ±5 minutes. This high synchronization hints at a feedback relationship between the CME and the flare energy release (Lin 2004; Zhang & Dere 2006; Maričić et al. 2007; Temmer et al. 2008, 2010; Reeves & Moats 2010). There are basically two forces acting on a

[3] This is a significantly higher rate than in the total sample of events, in which about 20% showed a double SXR peak.

flux rope in equilibrium, an upward-directed magnetic pressure and a downward-directed magnetic tension of the overlying magnetic field. When the magnetic structure loses equilibrium, it starts rising and a current sheet is formed below it, where magnetic reconnection takes place (Priest & Forbes 2002). The reconnection reduces the tension of the overlying field and enhances the magnetic pressure at the bottom part of the flux rope due to additional poloidal flux, providing the upward acceleration of the rope (Vršnak 2008). The upward motion of the rope leads to elongation of the current sheet and a more efficient reconnection, thus enhancing the acceleration. On the other hand, more efficient reconnection means also a more powerful energy release in the CME-associated flare, which directly relates the dynamics of the eruption and the energy release in the flare.

This work was supported by the Österreichische Förderungsgesellschaft (FFG) of the Austrian Space Applications Programme (ASAP) under grant no. 819664 and by the Fonds zur Förderung wissenschaftlicher Forschung (FWF): P20867-N16 and V195-N16. The *STEREO*/SECCHI data are produced by an international consortium of the Naval Research Laboratory (USA), Lockheed Martin Solar and Astrophysics Lab (USA), NASA Goddard Space Flight Center (USA), Rutherford Appleton Laboratory (UK), University of Birmingham (UK), Max-Planck-Institut für Sonnensystemforschung (Germany), Centre Spatiale de Liège (Belgium), Institut d'Optique Théorique et Appliquée (France), and Institut d'Astrophysique Spatiale (France).

REFERENCES

Bein, B. M., Berkebile-Stoiser, S., Veronig, A. M., et al. 2011, ApJ, 738, 191
Berkebile-Stoiser, S., Veronig, A. M., Bein, B. M., & Temmer, M. 2012, ApJ, 753, 88
Burkepile, J. T., Hundhausen, A. J., Stanger, A. L., St. Cyr, O. C., & Seiden, J. A. 2004, J. Geophys. Res. (Space Phys.), 109, 3103
Cheng, X., Ding, M. D., & Zhang, J. 2010, ApJ, 712, 1302
Cowan, G. 1998, Statistical Data Analysis (Oxford: Clarendon Press)
Dennis, B. R., & Zarro, D. M. 1993, Sol. Phys., 146, 177
Efron, B. 1979, Ann. Stat., 7, 1
Efron, B., & Tibshirani, R. 1986, Stat. Sci., 1, 54
Essenwanger, O. 1976, Applied Statistics in Atmospheric Science: Part A. Frequencies and Curve Fitting (Amsterdam: Elsevier Scientific Publishing Company)
Fletcher, L., Dennis, B. R., Hudson, H. S., et al. 2011, Space Sci. Rev., 159, 19
Gallagher, P. T., Lawrence, G. R., & Dennis, B. R. 2003, ApJ, 588, L53
Gopalswamy, N., Lara, A., Lepping, R. P., et al. 2000, Geophys. Res. Lett., 27, 145
Gopalswamy, N., Yashiro, S., Michalek, G., et al. 2009, Earth Moon Planets, 104, 295
Howard, R. A., Moses, J. D., Vourlidas, A., et al. 2008, Space Sci. Rev., 136, 67
Limbert, E., Stahel, A. W., & Abbt, M. 2001, Bioscience, 51, 341
Lin, J. 2004, Sol. Phys., 219, 169
Maričić, D., Vršnak, B., Stanger, A. L., & Veronig, A. 2004, Sol. Phys., 225, 337
Maričić, D., Vršnak, B., Stanger, A. L., et al. 2007, Sol. Phys., 241, 99
Michalek, G. 2009, A&A, 494, 263
Moon, Y.-J., Choe, G. S., Wang, H., et al. 2002, ApJ, 581, 694
Neupert, W. M. 1968, ApJ, 153, L59
Priest, E. R., & Forbes, T. G. 2002, A&AR, 10, 313
Reeves, K. K., & Moats, S. J. 2010, ApJ, 712, 429
Sachs, L. 1997, Angewandte Statistik, Anwendung statistischer Methoden (Berlin: Springer)
Temmer, M., Veronig, A. M., Kontar, E. P., Krucker, S., & Vršnak, B. 2010, ApJ, 712, 1410
Temmer, M., Veronig, A. M., Vršnak, B., et al. 2008, ApJ, 673, L95
Veronig, A., Vršnak, B., Dennis, B. R., et al. 2002, A&A, 392, 699
Veronig, A. M., Brown, J. C., Dennis, B. R., et al. 2005, ApJ, 621, 482
Vršnak, B. 2008, Ann. Geophys., 26, 3089
Vršnak, B., Maričić, D., Stanger, A. L., & Veronig, A. 2004, Sol. Phys., 225, 355
Vršnak, B., Maričić, D., Stanger, A. L., et al. 2007, Sol. Phys., 241, 85
Vršnak, B., Sudar, D., & Ruždjak, D. 2005, A&A, 435, 1149
Wuelser, J., Lemen, J. R., Tarbell, T. D., et al. 2004, Proc. SPIE, 5171, 111
Yashiro, S., & Gopalswamy, N. 2009, in IAU Symp. 257, Universal Heliophysical Processes, ed. N. Gopalswamy & D. F. Webb (Cambridge: Cambridge Univ. Press), 233
Yashiro, S., Gopalswamy, N., Michalek, G., et al. 2004, J. Geophys. Res. (Space Phys.), 109, 7105
Young, I. 1977, J. Histochem. Cytochem., 25, 935
Yurchyshyn, V., Yashiro, S., Abramenko, V., Wang, H., & Gopalswamy, N. 2005, ApJ, 619, 599
Zhang, J., & Dere, K. P. 2006, ApJ, 649, 1100
Zhang, J., Dere, K. P., Howard, R. A., Kundu, M. R., & White, S. M. 2001, ApJ, 559, 452
Zhang, J., Dere, K. P., Howard, R. A., & Vourlidas, A. 2004, ApJ, 604, 420